e and *Technology* contains non-
papers were reviewed by only the
rgo the usual peer review process
n the journal, *Fusion Science and*
re published as camera-ready and
the ANS editorial staff.

Transactions of Fusion Science and Technology

ISSN: 1536-1055

Transactions of Fusion Science and Technology

CONTENTS / FEBRUARY 2009—VOL. 55, NO. 2T

Proceedings of the

SEVENTH INTERNATIONAL CONFERENCE ON OPEN MAGNETIC SYSTEMS FOR PLASMA CONFINEMENT

Daejeon, Korea

July 15–18, 2008

[3] R. A. CAUSEY et al., J. Nucl. Material, **266-269** (1999) 467-471
[4] C. GARCIA-ROSALES et al., J. Nucl. Mater. **233-237** (1996)803-808.
[5]A.A. HASS et al., J. Nucl. Mater. **258-263** (1997)889-895.
[6] A.A. HASS et al., J. Nucl. Mater. **241-243** (1997)1076-1081.
[7] P. FRANZEN et al., J. Nucl. Mater. **241-243** (1997)1082-1086.
[8]V. KH.ALIMOV, B M. U. Scherzer **240** (1996)75-80.
[9]V. KH.ALIMOV, et al., **375** (2008)192-201.
[10] M. SAKAMOTO, et al., Nuclear Fusion **42** (2002) 165-168
[11] H. ZUSHI, et al, Nuclear Fusion **45** (2005) S142-S156
[12] R. BHATTACHARYAY, et al., Nuclear Fusion **47** (2007) 864-874.
[13] T. LOARER, Nucl. Fusion **47**, (2007) 1112-1120
[14] E. TITRONE, J. Nucl. Mater. **363-365** (2007)12-23.
[15] H. TAKENAGA, et al., Nucl. Fusion **46**, (2006) S39-S48.
[16] T. NAKANO, et al., Nucl. Fusion **46**, (2006) 626-634.
[17] Y. HIROOKA et al., J. Nucl. Mater. **363-365** (2007)775.
[18] H. IWAKIRI, et al., J. Nucl. Material, **307-311** (2002) 135-138
[19] K. TOKUNAGA et al., J. Nucl. Mater. **337-339** (2005)887.

TRANSPORT WITH REVERSED E_r IN THE GAMMA-10 TANDEM MIRROR

W. Horton, P. J. Morrison, X. R. Fu, J. Pratt
Institute for Fusion Studies, University of Texas at Austin, Austin, TX 78712, USA

The radial $E \times B$ transport losses in the central cell of the GAMMA-10 device are analyzed and compared with recent data from E_r-control experiments. Reversed E_r-profile are seen to inhibit transport.

I. ADVANTAGES OF THE TANDEM MIRROR FUSION SYSTEM

The GAMMA-10 tandem mirror system has achieved high energy confinement times ($70-90$ ms) with turbulent radial losses faster than the electrostatically- plugged end losses. The HIBP measured plug potentials give the Pastukhov end-loss time (100 ms). This high confinement time regime establishes a proof of principle that the combination of electrostatic and mirror confinement can successfully insulate electrons from thermal end losses. Tomography from the microchannel plates (MCP) with microsecond time resolution shows that a sheared radial electric field E_r suppresses the low frequency drift-wave fluctuations in the GAMMA-10. Radial energy confinement τ_E scaling laws derived in Pratt and Horton[1] provide a key prediction that there is a qualitatively different drift-wave turbulence in the tandem mirror geometry compared with toroidal systems.

There are three key advantages to a linear, open system as a fusion reactor over a toroidal systems. The most important advantage is that linear systems such as tandem mirrors possess no toroidal curvature, a significant consideration for confinement. Toroidal curvature produces instabilities on all spatial scales. MHD modes are stabilized in a toroidal system by keeping the plasma pressure small compared with the magnetic pressure, consequently there exists a β limit for each device. Some toroidal systems have relatively high beta ($\beta = L_p/Rq^2$) limits. The spherical tokamak has a large fraction of mirror-trapped particles and plasma betas approach 20%. Some large aspect ratio toroidal systems can have lower beta ($\beta = 2\mu_0 p/B^2$) limits. In contrast, the tandem mirror system has alternating regions of favorable and unfavorable curvature next to one another; this allows for a high beta limit of order unity. Small scale ion-temperature-gradient (ITG) and electron-temperature-gradient (ETG) modes in the torus are driven by the toroidal curvature and responsible for the toroidal scaling laws of Bohm and Gyro-Bohm confinement shown in Table I. Pratt and Horton[1] show that these laws can be developed in the context of a tandem mirror geometry and that a tandem mirror of comparable size to ITER could also produce $Q_{\text{fus}} = 10$.

A second major advantage of both the tandem mirror system and the helical system, over the tokamak design, for fusion power is that the confining magnetic fields are externally produced and controlled; in a tokamak the confining field is produced by a large, internal plasma current. The plasma current causes difficulties because it intrinsically attempts to produce magnetic reconnection to release its stored energy. Large plasma currents routinely cause major plasma disruption events at irregular intervals, as well as smaller sawteeth oscillations when either the plasma current is too large or the current profile is not optimal. In the ITER device a current of 15 MA is required to keep the alpha particle banana radius size below 0.3 m which is 15% of the minor radius. The device has aspect ratio $R/a = 6$ m/2 m and toroidal magnetic field $B_T = 5$ T. For the same length and field strength alpha particles in the linear mirror system would have gyroradius of 10 cm.

A third advantage to the linear open system is that there is a natural open divertor configuration. The escaping plasma can be allowed to expand over large areas, keeping the limits of the power-per-unit-area on material walls low. Escaping plasma can be configured to drive a direct energy conversion from plasma kinetic energy to electrical energy by separating the ion and electron orbits with a suitable system of electromagnetic fields. The principle of this direct conversion has been demonstrated on the GAMMA-10 device with the University of Kobe's bent-cusp direct convertor cell, which produces milliwatts of power per discharge[2]. These advantages of the linear, open system are well known. In this work, we investigate the theory of turbulent transport control in the context of the tandem mirror.

II. CONTROL OF THE RADIAL POTENTIAL PROFILES AND THE ASSOCIATED TRANSPORT CONTROL

The tandem mirror has a controlled ambipolar potential that varies along its length; this potential is produced through the use of electron cyclotron heating of the plug plasma and neutral beam injectors that create sloshing ion distributions in the barrier regions. The magnetic field on the right hand side of the machine is shown in Fig. 1 with each mirror cell labeled. With the proper injection of high-power-resonance electron-cyclotron heating from gyrotrons, a region of locally higher mean plasma potential $\Phi_0(r)$ is produced. The potential in the plasma is measured both with the heavy ion beam diagnostic and the electrostatic end loss analyzers.

Fig. 2 shows the experimental data and parameterized fits to these data from Cho *et al.*[3] for the electro-

TABLE I: Radial Loss Time Scaling Laws

$\tau_{L97} =$	.010	$B^{.99}$	$L^{.93}$	$a^{1.86}$	$n^{.4}$	$P^{-.73}$
$\tau_{H98} =$	.067	$B^{1.08}$	$L^{.46}$	$a^{2.44}$	$n^{.41}$	$P^{-.69}$
$\tau_{ISS95} =$	.080	$B^{.83}$	$L^{0.65}$	$a^{2.21}$	$n^{.51}$	$P^{-.59}$
$\tau_{ISS04} =$	.103	$B^{.89}$	$L^{.6}$	$a^{2.33}$	$n^{.59}$	$P^{-.64}$
$\tau_E^B =$	0.042	$B^{1/2}$	$L^{1/2}$	a^2	$n^{1/2}$	$P^{-1/2}$
$\tau_E^{gB} =$	0.016	$B^{.8}$	$L^{.6}$	$a^{2.4}$	$n^{.6}$	$P^{-.6}$
$\tau_E^{ETG} =$	.025	–	$L^{.33}$	$a^{2.66}$	n^1	$P^{-.33}$

static potential. The potential changes from monotonically decreasing (dashed curve) as a function of radius to a flattened non-monotonic profile (solid curve) with the injection of the electron cyclotron power creating a high energy electron ring in the region from $r = 4$ to 7 cm. This shape for the potential has been theoretically postulated, and found experimentally by the GAMMA-10 team[3]. The resulting maximum in radius of the electric potential $\Phi_0(r = 7\text{ cm}) \simeq 210$ V creates a reversed $E \times B$ rotation of the ions and electrons in the plasma. The flattened non-monotonic profile changes the drift wave transport because barriers to transport become robust and survive perturbation by the presence of fluctuations. Even in the case of weak perturbations, this behavior is signaled by the non-applicability of the standard Kolmogorov-Arnold-Moser (KAM) theorem[4] for Hamiltonian systems, which govern the motion of particles. However, of greater importance is the behavior of chaotic transport in such nontwist Hamiltonian systems under finite sized perturbations. The robustness of tori, barriers to transport, and diminished transport have been proposed[5] and investigated in general terms[6] and applied to a variety of experimental configurations e.g. Kwon *et al.*[7], and Marcus *et al.*[8].

III. MODELS OF THE RADIAL ELECTRIC FIELD AND THE ASSOCIATED $E \times B$ ORBITS

From Fig. 2 we have constructed the three analytic models shown in Fig. 3 with different features that may be within the error bars of the data from the HIBP and the electrostatic end-loss analyzers used to infer the internal plasma potential $\Phi_0(r)$. The models shown in Fig. 3 are:

1. Empirical model
   $\Phi_0(I^*) = -260I^*(I^*+1.49)(I^*-0.34)+205$, where $I^* = r^2/2a^2$.
2. Twist model
   $\Phi_0(I^*) = -460I^*(I^* - 0.33) + 205$.
3. Nontwist model
   $\Phi_0(I^*) = -700I^{*2}(I^* - 0.25) + 205$.

The ambipolar electric potential $\Phi_0(r, z)$ reflects the small pitch angle ions. For particles with small pitch

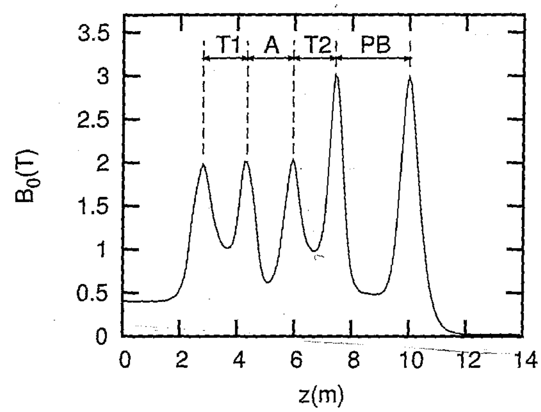

FIG. 1: The axial magnetic field on the right-hand-side of the GAMMA-10 tandem mirror. The central cell of the machine is situated at $z = 0$ and the left-hand-side of the axial magnetic field is symmetric. Labeled on the figure are transition region 1 (T1), the anchor region (A), transition region 2 (T2) and the plug-barrier region (PB).

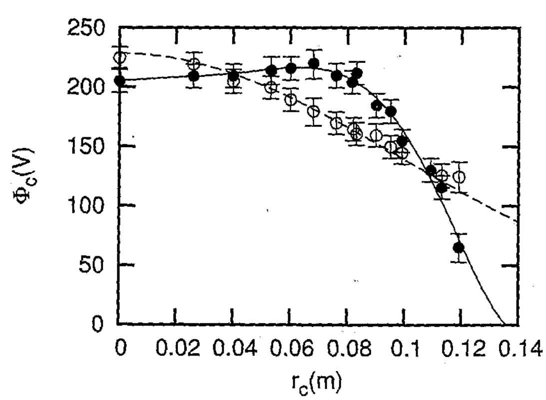

FIG. 2: Radial profile of electrostatic potential in the central cell from Cho *et al.*[3] Filled circles and the solid line represents the experimental data and a parameterized fit, respectively, with the injection of electron cyclotron heating; while hollow circles and the dashed line show results without injection of electron cyclotron heating.

TABLE I: Radial Loss Time Scaling Laws

$\tau_{L97} =$	.010	$B^{.99}$	$L^{.93}$	$a^{1.86}$	$n^{.4}$	$P^{-.73}$
$\tau_{H98} =$	.067	$B^{1.08}$	$L^{.46}$	$a^{2.44}$	$n^{.41}$	$P^{-.69}$
$\tau_{ISS95} =$	.080	$B^{.83}$	$L^{0.65}$	$a^{2.21}$	$n^{.51}$	$P^{-.59}$
$\tau_{ISS04} =$	.103	$B^{.89}$	$L^{.6}$	$a^{2.33}$	$n^{.59}$	$P^{-.64}$
$\tau_E^B =$	0.042	$B^{1/2}$	$L^{1/2}$	a^2	$n^{1/2}$	$P^{-1/2}$
$\tau_E^{gB} =$	0.016	$B^{.8}$	$L^{.6}$	$a^{2.4}$	$n^{.6}$	$P^{-.6}$
$\tau_E^{ETG} =$	.025	–	$L^{.33}$	$a^{2.66}$	n^1	$P^{-.33}$

static potential. The potential changes from monotonically decreasing (dashed curve) as a function of radius to a flattened non-monotonic profile (solid curve) with the injection of the electron cyclotron power creating a high energy electron ring in the region from $r = 4$ to 7 cm. This shape for the potential has been theoretically postulated, and found experimentally by the GAMMA-10 team[3]. The resulting maximum in radius of the electric potential $\Phi_0(r = 7\text{ cm}) \simeq 210$ V creates a reversed $E \times B$ rotation of the ions and electrons in the plasma. The flattened non-monotonic profile changes the drift wave transport because barriers to transport become robust and survive perturbation by the presence of fluctuations. Even in the case of weak perturbations, this behavior is signaled by the non-applicability of the standard Kolmogorov-Arnold-Moser (KAM) theorem[4] for Hamiltonian systems, which govern the motion of particles. However, of greater importance is the behavior of chaotic transport in such nontwist Hamiltonian systems under finite sized perturbations. The robustness of tori, barriers to transport, and diminished transport have been proposed[5] and investigated in general terms[6] and applied to a variety of experimental configurations e.g. Kwon *et al.*[7], and Marcus *et al.*[8].

III. MODELS OF THE RADIAL ELECTRIC FIELD AND THE ASSOCIATED $E \times B$ ORBITS

From Fig. 2 we have constructed the three analytic models shown in Fig. 3 with different features that may be within the error bars of the data from the HIBP and the electrostatic end-loss analyzers used to infer the internal plasma potential $\Phi_0(r)$. The models shown in Fig. 3 are:

1. Empirical model
$\Phi_0(I^*) = -260I^*(I^*+1.49)(I^*-0.34)+205$, where $I^* = r^2/2a^2$.

2. Twist model
$\Phi_0(I^*) = -460I^*(I^* - 0.33) + 205$.

3. Nontwist model
$\Phi_0(I^*) = -700I^{*2}(I^* - 0.25) + 205$.

The ambipolar electric potential $\Phi_0(r, z)$ reflects the small pitch angle ions. For particles with small pitch

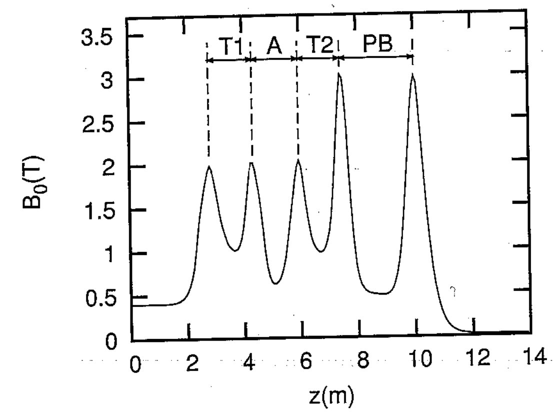

FIG. 1: The axial magnetic field on the right-hand-side of the GAMMA-10 tandem mirror. The central cell of the machine is situated at $z = 0$ and the left-hand-side of the axial magnetic field is symmetric. Labeled on the figure are transition region 1 (T1), the anchor region (A), transition region 2 (T2) and the plug-barrier region (PB).

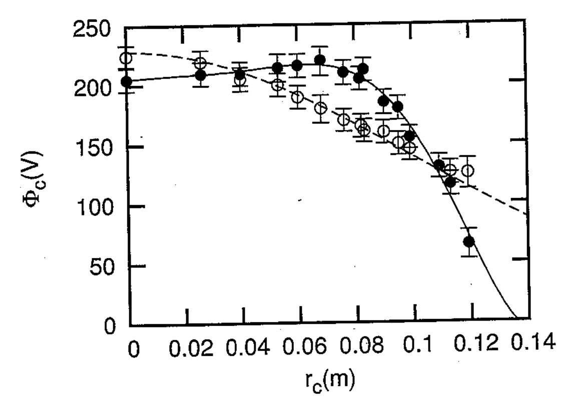

FIG. 2: Radial profile of electrostatic potential in the central cell from Cho *et al.*[3] Filled circles and the solid line represents the experimental data and a parameterized fit, respectively, with the injection of electron cyclotron heating; while hollow circles and the dashed line show results without injection of electron cyclotron heating.

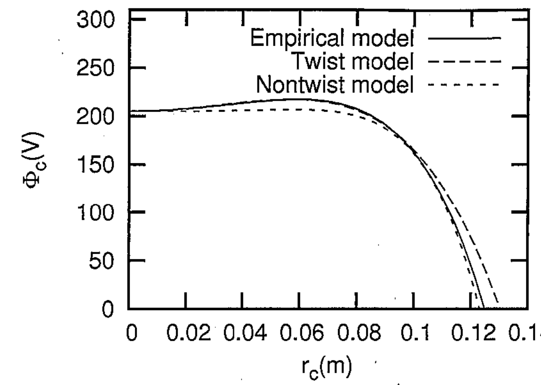

FIG. 3: Three analytic models for electrostatic potential in the central cell constructed from the data of Cho *et al.*[3] in Fig. 2.

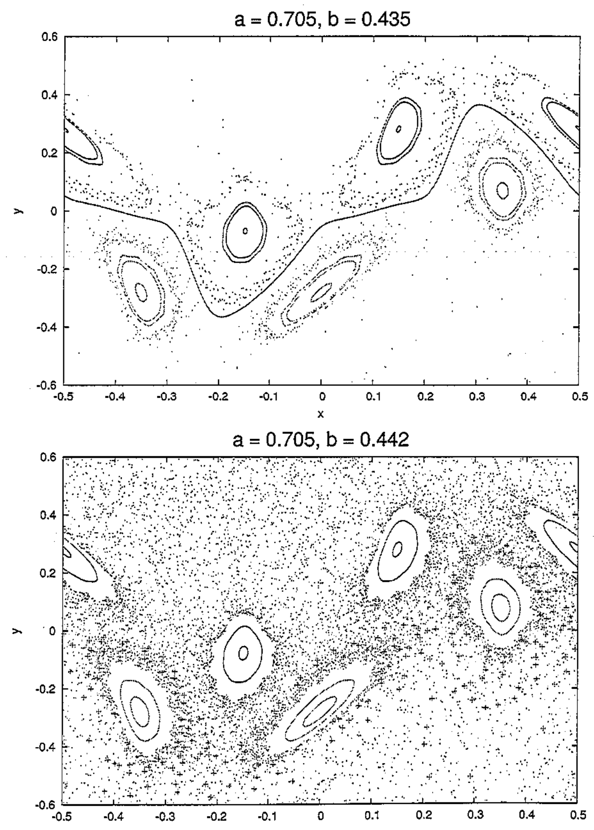

FIG. 4: Surface-of-section in the $I-\theta$ plane of the $E \times B$ orbits inside and outside the last invariant surface arising from the reversed E_r(top) and after the surface is broken(bottom).[9,10]

angles, $\mu = mv_\perp^2/2B \ll \epsilon/B$, the parallel motion is given by the Lagrangian $L = mv_\parallel^2/2 - q\Phi(z)$, where

$$\frac{dz}{dt} = v_\parallel \tag{1}$$

$$\frac{dv_\parallel}{dt} = -\frac{q}{m}\frac{\partial\Phi}{\partial z}. \tag{2}$$

Particles bouncing at a typical frequency $\omega_b \sim v_\parallel/2L_{cc} \sim 5\times10^4\ \text{s}^{-1}$, can resonate with drift waves whose frequency $\omega_k = mT_e/reBL_n$, where L_n is the density gradient scale length.

IV. DRIFT WAVE SPECTRUM

For drift waves, many modes can exist, thus the total potential in cylindrical coordinates is

$$\Phi(r,\theta) = \Phi_0(r) + \sum \phi_m(z)\cos(m\theta - \omega_k t + \xi_m), \tag{3}$$

where $\phi_m = \phi_1 m^{-\alpha_m}$, with spectral index $\alpha_m = 1$ or 2, and the phase ξ_m is a random value between 0 and 2π.

To start with, we can choose $\phi_m(z) = \text{const}^{11}$, i.e. a flute mode in which $\mathbf{B}\cdot\nabla\Phi = 0$. The guiding center motion is generated by

$$\frac{d\mathbf{x}}{dt} = \frac{\mathbf{E}\times\mathbf{B}}{B^2} = \left(\frac{-1}{rB}\frac{\partial\Phi}{\partial\theta}, \frac{1}{B}\frac{\partial\Phi}{\partial r}, 0\right). \tag{4}$$

By defining $I = r^2/2$, we get the Hamiltonian structure

$$\frac{dI}{dt} = -\frac{1}{B}\frac{\partial\Phi}{\partial\theta} \tag{5}$$

$$\frac{d\theta}{dt} = \frac{1}{B}\frac{\partial\Phi}{\partial r}, \tag{6}$$

with the Hamiltonian $H = \Phi/B$, momentum I, and coordinate θ.

Based on Fig. 2, we try two models for $E_r = -d\Phi_0(r)/dr$:

1. E_r points outward
We record the time for particles to escape(so called "first exit time"), i.e. $x^2(t_{\text{exit}}) + y^2(t_{\text{exit}}) = 2I > a^2$.

2. Reversed E_r experiment
From Fig. 2 and 3, we have $I_{\text{crit}} = a^2/4$, i.e. $r_c = .707a$, $a = 10$ cm. There exists a reversal layer at a radius of r_c. Outside the layer, E_r points outward, while inside E_r points inward. At the reversal layer,

$$\Omega(r_c^2) = \frac{-E_r}{rB} \to 0$$

$$= \frac{1}{rB}\frac{d\Phi}{dr} = \frac{1}{B}\frac{d\Phi}{dI}, \tag{7}$$

$$\dot\theta = dH/dI. \tag{8}$$

Integration of ensembles show that the reversed layer results in a large increase in the average first exit time.

From simulations and data we note that a dominant single mode $\phi = \phi_m\cos(m\theta - \omega t)$ gives islands in the $I-\theta$ phase plane. For the case when many waves are present, $\phi = \sum\phi_m\cos(m\theta - \omega t + \xi_m)$, the islands overlap and Hamiltonian motion transitions to a stochastic diffusive motion.

V. ONSET OF CHAOTIC DIFFUSION

In Fig. 4, taken from Horton *et al.*[9](see also Apte *et al.*[10]), the phase space shows that in these type of systems there exists a transport barrier for the nontwist potential profile such as model 3 with fluctuating voltages up to $\phi \sim 4$ V. For the twist map in model 2 the last integral curve producing the transport barrier breaks down at a smaller fluctuating potential $\phi \leq 1$ V. For fluctuating potentials greater than 10 V there is a radial diffusive transport $D(\phi)$ as in quasi-linear theory. However the level of $D(\phi)$ remains lower with the nontwist potential profile. A similar effect is observed in tokamak edge dynamics[8].

High speed photographs of the Balmer alpha line (656 nm) from the $n = 3$ to 2 transitions of the atomic hydrogen in the central cell of the GAMMA-10 by Nakashima *et al.*[12] show the speed up and then collapse of the plasma pressure. The plasma rotates in the ion diamagnetic direction at 9 to 10 kHz corresponding to the $m = 1$ mode in the collapse of the plasma pressure. During the growth of the image signal before the collapse one sees briefly what appears to be the $m = 2$, 3 and 4 distortions in the images (`http://pecos.ph.utexas.edu/~vortex`). For the rotational instabilities, the basic results for the $m = 1$ and 2 modes for the tandem mirror geometry are given in detail by Liu *et al.*[13]

The rotational stability theory depends on the details of the E_r and ion pressure profiles as well as the ratio of the radius of the conducting wall divided by the radius of the hot plasma. For $m = 1$ the growth rate increases as the conducting wall moves inward to the plasma in contrast to $m = 2$ where the close wall is stabilizing. This is because the $m = 1$ is a displacement mode that is neutrally stable in the absence of a conducting wall. With the conducting wall the Dirichlet boundary condition induces an image charge in the wall that makes an effective dipolar structure that is unstable. The $m = 1$ mode, called the wobble mode, contains the dominant energy component of the nonlinear state in the late stages of the nonlinear evolution. These early theoretical results are confirmed by the high speed CMOS/CCD camera movies.

VI. CONCLUSION

The radial plasma losses are controlled by the E_r-profile in the linear tandem mirror system. Both theory and the experiment show that a reversal of the E_r-profile reduces the radial transport. The core ion pressure then increases. The increasing pressure gradient finally results in a plasma disruption as seen in the Balmer α emission and the drop in the diamagnetic signal.

REFERENCES

[1] J. Pratt and W. Horton, *Physics of Plasmas* **13**, 042513 (2006).
[2] Y. Yasaka, T. Yamamoto, Y. Kurumatani, H. Takeno, Y. Nakashima, T. Cho, Y. Tomita, and M. Ishikawa, *Nuclear Fusion* **48**, 035015 (2008).
[3] T. Cho, V. P. Pastukhov, W. Horton, T. Numakura, M. Hirata, J. Kohagura, N. V. Chudin, and J. Pratt, *Physics of Plasmas* **15**, 056120 (2008).
[4] J. V. José and E. J. Saletan, *Classical Dynamics: A Contemporary Approach*, Cambridge University Press, 1998.
[5] D. del-Castillo-Negrete and P. J. Morrison, *Physics of Fluids* **5**, 948 (1993).
[6] D. del-Castillo-Negrete, J. M. Greene, and P. J. Morrison, *Physica D Nonlinear Phenomena* **100**, 311 (1997).
[7] J.-M. Kwon, W. Horton, P. Zhu, P. J. Morrison, H.-B. Park, and D. I. Choi, *Physics of Plasmas* **7**, 1169 (2000).
[8] F. A. Marcus, I. L. Caldas, Z. O. G. aes Filho, P. J. Morrison, W. Horton, Y. K. Kuznetsov, and I. C. Nascimento, (2008), Submitted to *Physics of Plasmas.*
[9] W. Horton, H. V. Wong, P. J. Morrison, A. Wurm, J. H. Kim, J. C. Perez, J. Pratt, G. T. Hoang, B. P. LeBlanc, and R. Ball, *Nuclear Fusion* **45**, 976 (2005).
[10] A. Apte, A. Wurm, and P. J. Morrison, *Chaos* **13**, 421 (2003).
[11] W. Horton, J. Liu, J. D. Meiss, and J. E. Sedlak, *Physics of Fluids* **29**, 1004 (1986).
[12] Y. Nakashima, N. Nishino, Y. Higashizono, H. Kawano, S. Kobayashi, M. Shoji, Y. Kubota, M. Yoshikawa, M. K. Islam, Y. Mishima, D. Mimura, and T. Cho, *Journal of Nuclear Materials* **363**, 616 (2007).
[13] J. Liu, W. Horton, and J. E. Sedlak, *Physics of Fluids* **30**, 467 (1987).